Vol. 14 No. 2 (2023) 45-53

Jurnal Riset
Teknologi Pencegahan Pencemaran Industri

Journal homepage : https://www.jrtppi.id

Kementerian Perindustrian
REPUBLIK INDONESIA

Easy Preparation of Zinc Molybdate Photocatalyst ($ZnMoO_4$) and Its Application for Degradation of Methylene Blue

Ridla Bakri*[1], Rika Firmansyah[1], Yoki Yulizar[1]

[1] Department of Chemistry, Universitas Indonesia.

ARTICLE INFO

Article history:
Received January 11, 2023
Received in revised form January 20, 2023
Accepted April 26, 2023
Available online November 10, 2023

Keywords :
Methylene Blue
Organic Pollutant
Photocatalyst
Zinc Molybdate

ABSTRACT

Using photocatalyst is one way to overcome the problem of dye waste in water. Hazardous chemicals are commonly used in the manufacture of photocatalysts. In this research, $ZnMoO_4$ was prepared through an environmentally friendly and cost-effective synthesis. $ZnMoO_4$ was synthesized using peppermint leaf extract. The alkaloid content of the leaf extract was hydrolysed to form hydroxy ions. Subsequently, the hydroxyl ions were subjected to a hydrothermal process, resulting in the formation of $ZnMoO_4$. The functional groups, crystalline structure and morphology of $ZnMoO_4$ were characterised using fourier transform infrared (FTIR), X-ray diffraction (XRD), field emission scanning electron microscopy (FE-SEM), and transmission electron microscopy (TEM). The band gap energy was investigated through UV-Vis diffuse reflectance spectroscopy (UV-Vis DRS). The photocatalytic activity of $ZnMoO_4$ was tested against the organic pollutant methylene blue under visible light irradiation and its degradation products were analysed with a UV-Vis spectrophotometer at a wavelength of 664 nm. After 80 minutes of irradiation, the photocatalytic process of $ZnMoO_4$ degraded 99% of methylene blue. The excellent photodegradation performance suggests that the transition activity of electron currents from the valence band to the conduction band on $ZnMoO_4$ is occurring effectively.

1. INTRODUCTION

Methylene blue (MB) is commonly used in the textile, paper and paint industries (Pham et al., 2021; Riwayati, Fikriyyah, & Suwardiyono, 2019; Simi & Azeeza, 2010). The presence of methylene blue in water is a pollutant that is harmful to humans (Ken Gillman, 2011; Radoor, Karayil, Jayakumar, Parameswaranpillai, & Siengchin, 2021). Photocatalysis is one of the treatment methods for dye wastewater (Sagadevan et al., 2022; Sirirerkratana, Kemacheevakul, & Chuangchote, 2019). The basis of photocatalysis is the use of light to excite electrons to form photogenerated electron-hole pairs and initiate redox reactions on the surface of the photocatalyst (Low, Yu, Jaroniec, Wageh, & Al-Ghamdi, 2017). Metal oxide semiconductors with a wide band gap act as photocatalysts under UV light, while metal oxides with a narrow band gap adsorb visible light (Astuti, Listyani, Suyati, & Darmawan, 2021; Meng et al., 2017; Widiyandari, Ketut Umiati, & Dwi Herdianti, 2018). Sunlight with a high visible light content can be used as a photocatalytic light source (Liebel, Kaur, Ruvolo, Kollias, & Southall, 2012; Wang et al., 2018). Therefore, narrow bandgap semiconductors are needed to optimise the use of visible light from sunlight.

$ZnMoO_4$ is a non-toxic oxidation metal commonly used as anode material (Fei et al., 2017; Zhang, Feng, Liu, & Guo, 2019), catalyst (Petrović et al., 2021), anti-bacterial (Mardare, Tanasic, Rathner, Müller, & Hassel, 2016), and

*Correspondence author.
E-mail : ridla.bakri@sci.ui.ac.id (Ridla Bakri)

doi : https://10.21771/jrtppi.2023.v14.no.2.p45-53
2503-5010/2087-0965© 2021 Jurnal Riset Teknologi Pencegahan Pencemaran Industri-BBSPJPPI (JRTPPI-BBSPJPPI).
This is an open acces article under the CC BY-NC-SA license (https://creativecommons.org/licenses/by-nc-sa/4.0/).
Accreditation number : (Ristekdikti) 158/E/KPT/2021

anti-corrosion (Xing, Xu, Wang, & Hu, 2019) as well as photocatalyst (Chen, Zhang, Yang, Yang, & Sun, 2021; Yan et al., 2019). β-$ZnMoO_4$ has a monoclinic phase system with Zn and Mo atomic bonds attached to 6 oxygen atoms and can adsorb visible light. It is a metastable material that transforms into α-$ZnMoO_4$ at high temperatures (Ait Ahsaine et al., 2016). The production of $ZnMoO_4$ usually uses chemicals such as NaOH base, which are harmful to the environment (Lv, Tong, Zhang, Su, & Wang, 2011).

Indonesia is renowned for its rich biodiversity and vast plant species, which hold immense potential in the development of green synthesis methods. The development of green synthesis methods in this research aims to reduce the use of hazardous and toxic materials. In this paper, fabrication of $ZnMoO_4$ was carried out by green synthesis using peppermint leaves extract. Peppermint contains secondary metabolites such as flavonoids, tannins, saponins and alkaloids. (Fialová et al., 2014; Puspitasari, Mareta, & Thalib, 2021). The content of alkaloids can replace the use of the starting NaOH material, while flavonoids, tannins, and saponins can be used as capping agents that can maintain the formation of nanoparticles so that they are stable to form nanoparticles (Weldegebrieal, 2020; Yulizar, Apriandanu, & Ashna, 2020; Yulizar, Bakri, Apriandanu, & Hidayat, 2018).

2. MATERIAL AND METHODS

2.1. $ZnMoO_4$ Synthesis

To obtain secondary metabolites in peppermint leaves, dry and clean leaves were macerated with methanol in a ratio of 1:5 (g/v). The filtrate was added with n-hexane in a ratio of 1:1 (v/v) and then separated. The resulting solution of the methanol fraction was concentrated to thickening using a vacuum rotary evaporator. The viscous liquid is dissolved in water as peppermint extract (PE) and stored in the refrigerator.

Stirred for 10 minutes with 5 mL of $(NH_4)_6Mo_7O_{24}.4H_2O$ and $Zn(NO_3)_2.4H_2O$ at a ratio of 0.15 mmol and 1.05 mmol, respectively. Into the mixture then added 1 mL of peppermint extract (PE) and stirred it for 30 minutes. The stirred mixture was placed in a 25-mL Teflon autoclave chamber and then heated in an oven at 160°C for 6 hours. Cool the autoclave to room temperature. The precipitate formed was washed with distilled water and methanol three times each and then heated at 80°C for 3 hours until a light grey powder was formed.

2.2. Material Characteristics

To prove that the synthesized catalyst is $ZnMoO_4$, the catalyst was characterized using various instruments. X-ray diffraction (XRD) Shimadzu 2700 was used to analyse the structure of the nanoparticles, the Fourier Transform Infrared (FTIR) Shimadzu Prestige 21 was used to determine functional groups, DRS UV-vis Spectrophotometer Agilent Technologies Carry 60 was used to test band gap, field emission - scanning electron microscopy spectroscopy (FESEM-EDX) JEOL JIB-4610F and Transmission Electron Microscope (TEM) - Tecnai 200 kV D2360 was used to see the morphology and atomic composition.

2.3. Photocatalytic Activity of $ZnMoO_4$

8 mg ZnMoO4 powder were added to 50 mL of 1x10-5 M methylene blue (MB) solution with constant stirring under visible light (125 W lamp, λ 420 nm, Philips) for 80 minutes. The degradation of the MB solution that occurred was measured using an Agilent Cary 100 UV-Vis Spectrophotometer at a wavelength of 664 nm. The calculation of the percentage degradation of MB is done by the equation:

$$\%\ degratation = \frac{A_0 - A_t}{A_0} \times 100\%$$

where A_0 is the initial concentration of MB dye and A_t is the residual concentration of MB.

3. RESULT AND DISCUSSION

3.1. Characterization Material

A phytochemical screening of peppermint leaves extract was carried out based on a previous study by Dwi, Anam, & Kusrini (2016). Table shows the result of the phytochemical test. It revealed the presence of secondary metabolites in methanol fractions such as alkaloids, flavonoids, tannins, and saponins. The phytochemical

results of the n-hexane fraction did not contain secondary metabolites of alkaloids, flavonoids, tannins, and saponins. This indicates that the secondary metabolites used are polar.

FTIR tests were also performed to determine the functional groups in the peppermint extract. The results of the FTIR test can be seen in Figure 1(a). The presence of a spectrum at wave number 1643 cm-1 indicates the presence of the NH functional group, which indicates alkaloids in the sample. A wide peak with a maximum peak at a wavelength 3331 cm-1 indicates the presence of a hydroxy functional group (-OH), which is part of the flavonoids, tannins, and saponins.

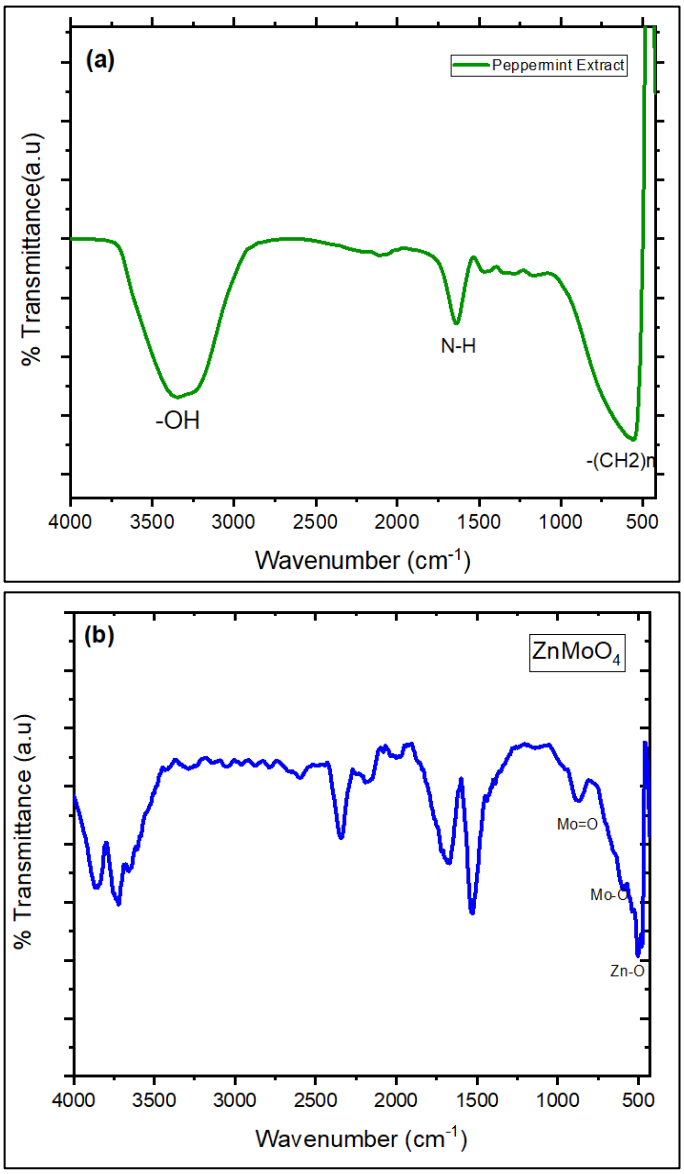

Figure 1. FTIR Spectra of (a) Peppermint Extract and (b) $ZnMoO_4$

Table 1. Result of Phytochemical Test

Metabolic Secondary	n-Hexane Fraction	Methanol fraction
Alkaloid	-	+
Flavonoid	-	+
Tannin	-	+
Saponin	-	+

FTIR spectra in Figure 1(b) show the presence of ZnO bonds at 489 cm^{-1} (Bharathi, Sivakumar, Udayabhaskar, Takebe, & Karthikeyan, 2014), as well as Mo-O bonds at 609 and 882 cm^{-1} (Reddy, Vickraman, & Justin, 2018). The presence of wave numbers at 1500-4000 indicate the presence of organic compounds derived from residual secondary metabolites still bound to ZnMoO4. Spectra in the 1500-2000 ranges are regional triple bonds for C=N, C=C and C=O; 2000-2500 ranges are regional triple bonds for C≡C and C≡N while 2500-4000 are regional single bonds for the C-H group and O-H (Nandiyanto, Oktiani, & Ragadhita, 2019).

The alkaloid compounds in the leaf extract will be hydrolysed in water to form OH- bases, which will react with metal ions Zn^{2+} and $(Mo_7O_{24})^{6-}$ to form hydroxy compounds. By the pressure in the hydrothermal process these hydroxy compounds will form metal oxide $ZnMoO_4$. Meanwhile, the presence of other secondary metabolites such as flavonoids, saponins, and tannins, act as a capping agent that maintains the stability of particle formation. The reaction between alkaloids and metal ions is shown in the following reactions:

$$Zn(NO_3)_2.4H_2O_{(s)} \rightarrow Zn^{2+}{}_{(aq)} + 2NO_3^-{}_{(aq)} + 4H_2O_{(l)} \quad (1)$$

$$(NH_4)6Mo_7O_{24}.4H_2O_{(s)} \rightarrow 6NH_4^+{}_{(aq)} + Mo_7O_{24}^{6-}{}_{(aq)} + 4H_2O_{(l)} \quad (2)$$

$$R_2\text{-}N\text{-}CH_{3\,(aq)} + H_2O_{(l)} \rightleftharpoons R_2\text{-}N{+}H\text{-}CH_{3\,(aq)} + OH^-{}_{(aq)} \quad (3)$$

$$7\ Zn^{2+}{}_{(aq)} + Mo_7O_{24}^{6-}{}_{(aq)} + OH^-{}_{(aq)} \rightarrow 7\ ZnMoO_{4(s)} + 4\ H_2O_{(l)} \quad (4)$$

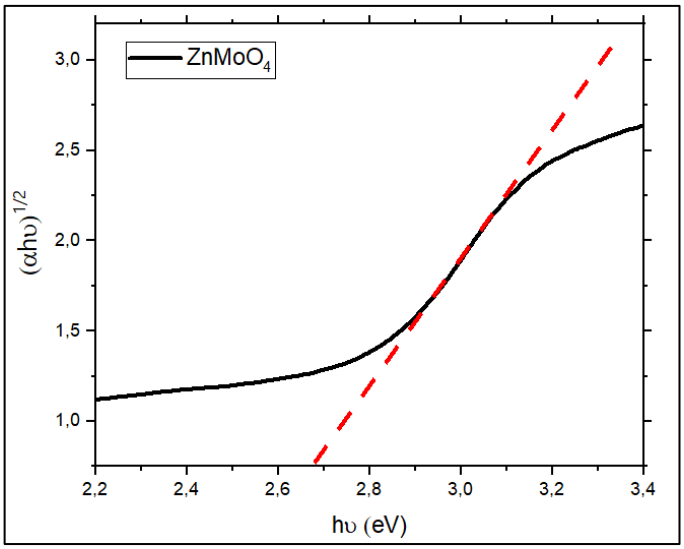

Figure 2. Bandgap Energy of $ZnMoO_4$

The estimated bandgap energy of ZnMoO4 was determined using the Tauc Plot equation as follows:

$$\alpha h\upsilon = A(h\upsilon - Eg)^{1/2}$$

where α is absorption coefficient, h is Planck's constant, υ is the frequency of light, Eg is energy bandgap, and A is a constant number. By plotting $(\alpha h\upsilon)^{1/2}$ and hυ into a graph, and extrapolating $(\alpha h\upsilon)^{1/2} = 0$ linearly, one can estimate the energy value Eg of the bandgap. As shown in Figure 2, the energy of the bandgap of $ZnMoO_4$ is 2.67 eV. This result shows that the electrons of $ZnMoO_4$ are easily excited by visible light (Jiang et al., 2014; Lv et al., 2011).

The diffraction patterns of $ZnMoO_4$, shown in Figure 3, were analysed by XRD. In the $ZnMoO_4$ diffraction pattern with a value of 2θ is 18.64; 24.16; 30.24; 30.96; 36.01; 36.35; 38.10; 40.99; 44.32; 48.56; 49.96; 51.31;53.63; 53.96; 54.78. Meanwhile, those indexed on PDF2 00-016-0310 have a value of 2θ which corresponds to the Miller index (100), (110), (-111), (020), (021), (120), (200), (210), (-112), (022), (220), (130), (-221), (202), and (-131) and has a monoclinic phase form.

FE-SEM EDX analysis was used to investigate the morphology and elemental composition of $ZnMoO_4$. Figure 4(a-b) depicts the morphology of $ZnMoO_4$ at different magnifications, resulting in non-uniform agglomerated flakes. EDX mapping analysis of $ZnMoO_4$ is shown in Figure 4(c-d). The mapping results show that the elements Zn, Mo, and O are distributed evenly. The results of the EDX elemental composition calculation are shown in Figure 4(e), where the atomic compositions of Zn, Mo, and O are 17%, 14%, and 69%, respectively. This corresponds to the original mole number of the synthesis with a mole ratio of 1:1:4 for $ZnMoO_4$. The results of TEM are shown in Figure 5. The SEM and TEM images show a variety of particle sizes with relatively the same shape, namely flakes. This indicates that the formation of $ZnMoO_4$ has been successfully synthesised.

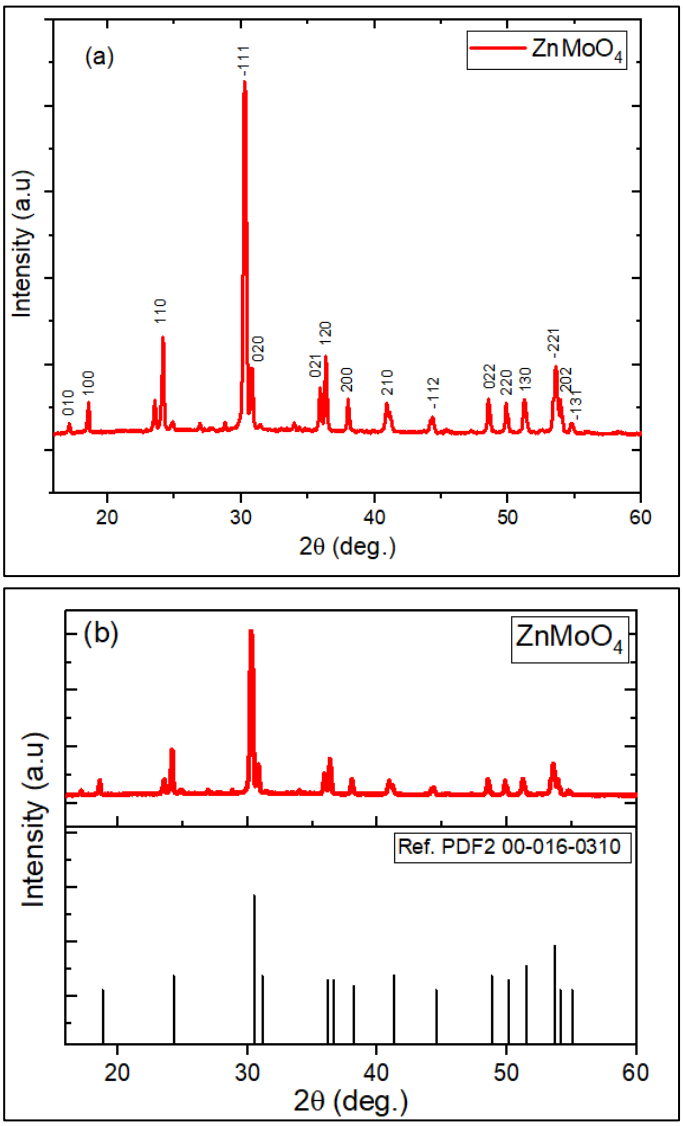

Figure 3. XRD Pattern of (a) $ZnMoO_4$ (b) $ZnMoO_4$ dan Index Miller (b) $ZnMoO_4$ and Ref. PDF2 00-016-0310

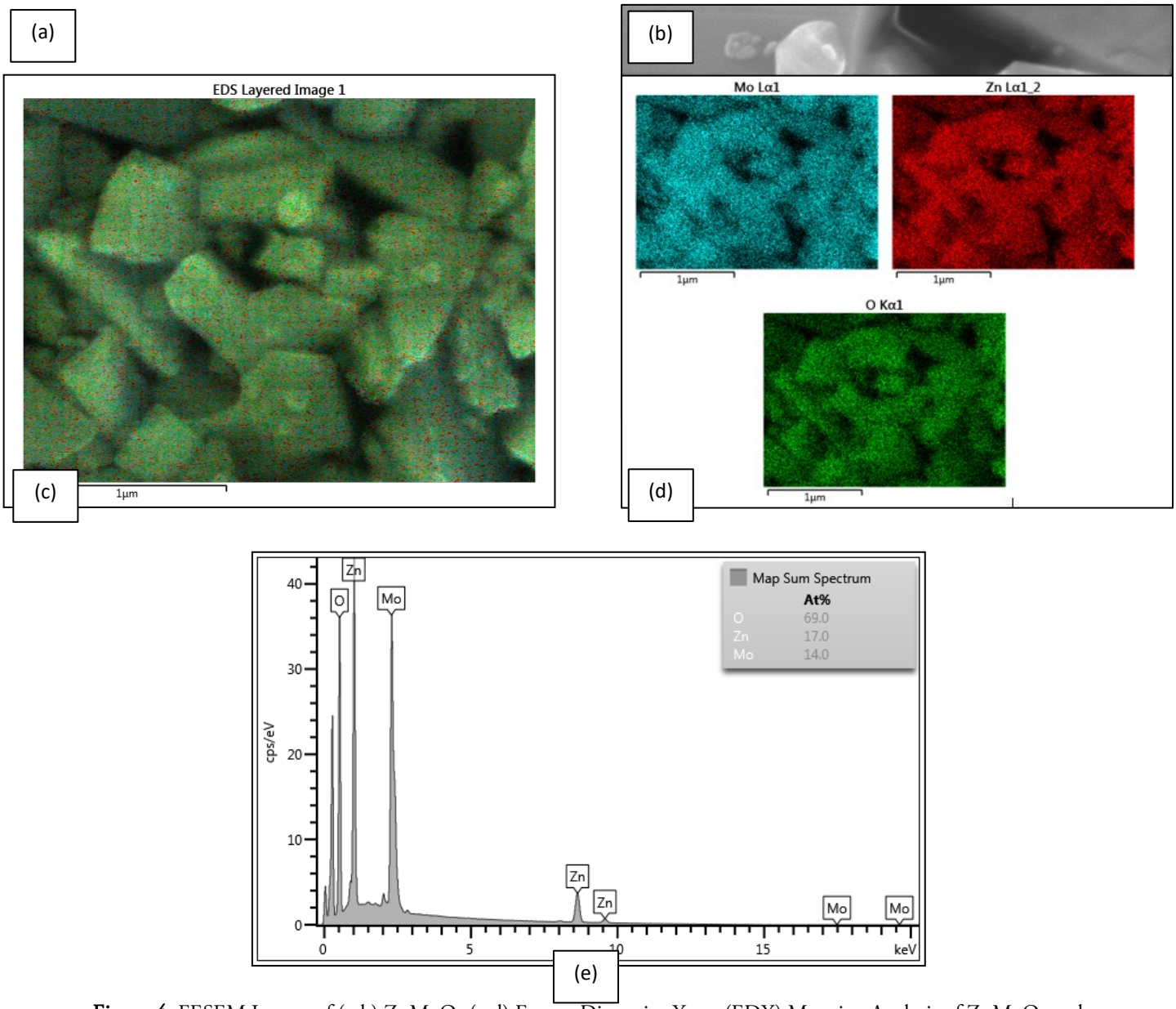

Figure 4. FESEM Images of (a-b) $ZnMoO_4$ (c-d) Energy Dispersive X-ray (EDX) Mapping Analysis of $ZnMoO_4$ and (e) EDX Spectrum of $ZnMoO_4$

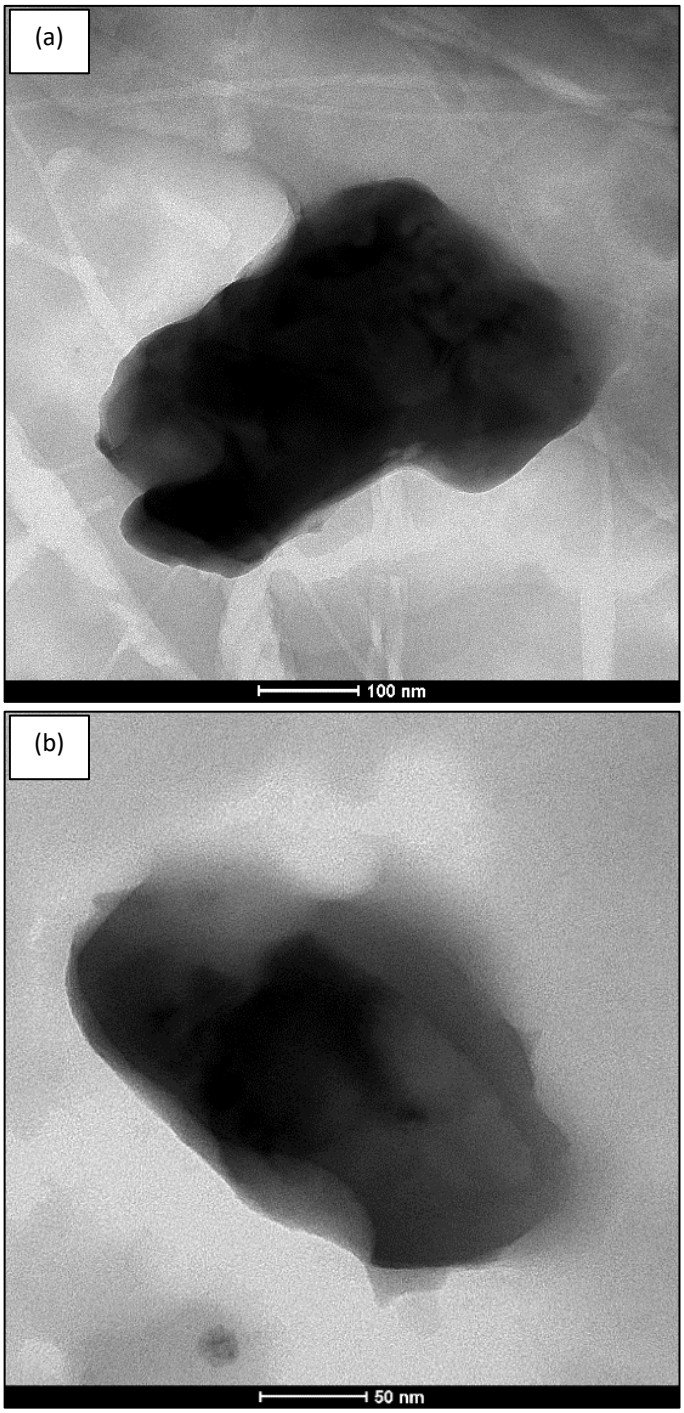

Figure 5. TEM Images of $ZnMoO_4$ (a) 100 nm scale (b) 50 nm scale

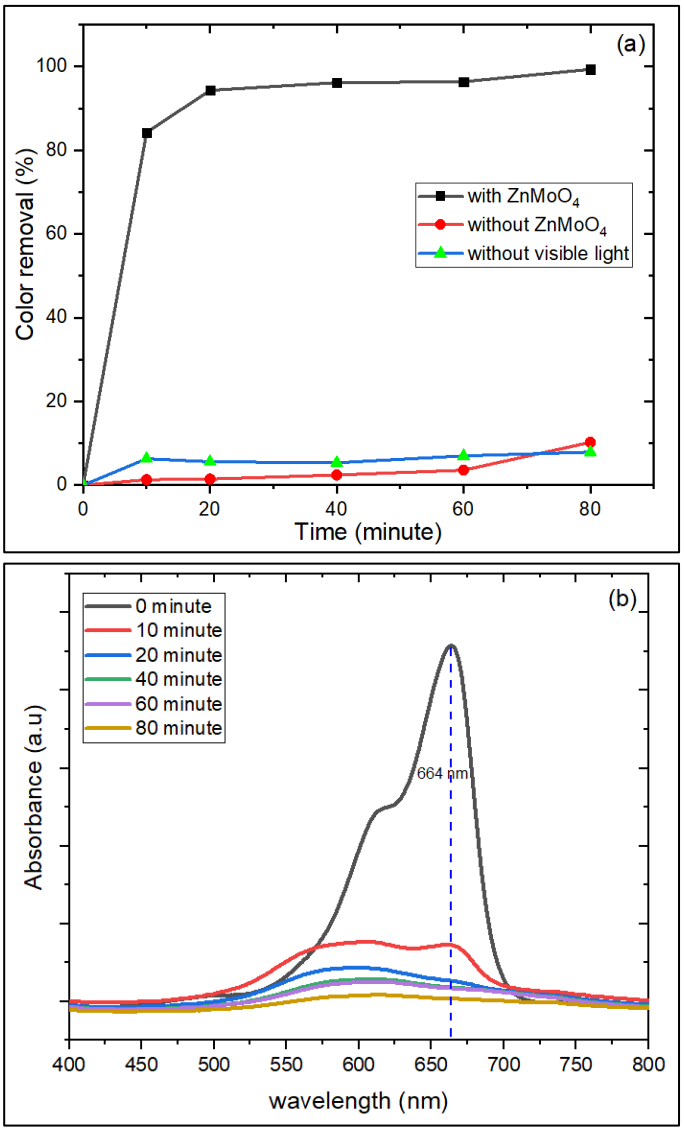

Figure 6. (a) % Degradation of Methylene Blue (MB) (b) Spectra Spectrophotometric Uv-Vis of MB Degradation by $ZnMoO_4$

3.2. Performance of Photocatalytic Degradation

A photocatalytic test was performed on irradiated MB under visible light. Figure 6(a) shows the degradation of methylene blue (MB) by $ZnMoO_4$ under visible light reaches 99.3%, whereas degradation of MB without $ZnMoO_4$ is only 10.4% and the degradation in the absence of visible light is about 7.90%. The process without visible light indicates the presence of dye adsorption by the catalyst. This adsorption process is relatively small compared to the degradation of dyes, that reaches 99%. Therefore, the degradation of MB is affected by the photocatalytic process. Photocatalysis is triggered by visible light, that is adsorbed

by $ZnMoO_4$ and excites electrons. This photogeneration process produces electron (-) in the conduction band (ecb^-) and holes (+) in the valence band (hvb^+). The electrons react with O_2 to form superoxide radicals ($O_2\bullet^-$), meanwhile, the holes in the valence band react with OH^- / H_2O to form hydroxy radicals (•OH). These hydroxy radicals, along with the superoxide radicals ($O_2\bullet^-$) produced by the electrons in the conduction band, react with MB to degrade it into H_2O and CO_2. Figure 6(b) is the uv vis spectrophotometer spectra of MB degradation by $ZnMoO_4$ catalyst for 80 min. From the figure it can be seen the absorbance decrease at a maximum wavelength of 664 nm. This decrease is due to the photocatalytic process which degrades MB into simpler compounds. The reaction:

$$ZnMoO_4 + h\upsilon \rightarrow ZnMoO_4\,(ecb^- + h\upsilon b^+) \quad (5)$$

$$h\upsilon b^+ + OH^- \rightarrow \bullet OH \quad (6)$$

$$ecb^- + O_2 \rightarrow O_2\bullet^- \quad (7)$$

$$O_2\bullet^- + H_2O \rightarrow HO_2\bullet + OH^- \quad (8)$$

$$HO_2\bullet + HO_2\bullet \rightarrow H_2O_2 + O_2 \quad (9)$$

$$H_2O_2 + O_2\bullet^- \rightarrow \bullet OH + OH^- + O_2 \quad (10)$$

$$\bullet OH + O_2\bullet^- + MB \rightarrow CO_2^- + H_2O \quad (11)$$

4. CONCLUSION

The facile preparation of $ZnMoO_4$ photocatalyst has been successfully synthesized by using environmentally friendly natural materials. The synthesis of $ZnMoO_4$ by green synthesis has a morphology in the form of flakes and the shape of the phase system formed is monoclinic. The bandgap of $ZnMoO_4$ is 2.67 eV, which makes it active as a photocatalyst under visible light. Photodegradation of methylene blue by $ZnMoO_4$ under visible light showed very good results, with the colour degradation rate reaching 99%.

ACKNOWLEDGMENT

Financial support for this research comes from LPDP Indonesia.

REFERENCE

Ait Ahsaine, H., Zbair, M., Ezahri, M., Benlhachemi, A., Bakiz, B., Guinneton, F., & Gavarri, J. R. (2016). Structural and Temperature-dependent vibrational analyses of the non-centrosymmetric ZnMoO4 molybdate. Journal of Materials and Environmental Science, 7(9), 3076-3083.

Astuti, Y., Listyani, B. M., Suyati, L., & Darmawan, A. (2021). Bismuth oxide prepared by sol-gel method: Variation of physicochemical characteristics and photocatalytic activity due to difference in calcination temperature. Indonesian Journal of Chemistry, 21(1), 108-117.https://doi.org/10.22146/ijc.53144

Bharathi, V., Sivakumar, M., Udayabhaskar, R., Takebe, H., & Karthikeyan, B. (2014). Optical, structural, enhanced local vibrational and fluorescence properties in K-doped ZnO nanostructures. Applied Physics A: Materials Science and Processing, 116(1), 395-401. https://doi.org/10.1007/s00339-013-8139-8

Chen, P., Zhang, Z., Yang, S., Yang, Y., & Sun, Y. (2021). Synthesis of BiOCl/ZnMoO4 heterojunction with oxygen vacancy for enhanced photocatalytic activity. Journal of Materials Science: Materials in Electronics, 32(18), 23189-23205. https://doi.org/10.1007/s10854-021-06805-6

Dwi, J., Anam, K., & Kusrini, D. (2016). Penentuan Total Kadar Fenol dari Daun Kersen Segar, Kering dan Rontok (Muntingia calabura L.) serta Uji Aktivitas Antioksidan dengan Metode DPPH. Jurnal Kimia Sains Dan Aplikasi, 19(1), 15-20 https://doi.org/10.14710/jksa.19.1.15-20

Fei, J., Sun, Q., Li, J., Cui, Y., Huang, J., Hui, W., & Hu, H. (2017). Synthesis and electrochemical performance of α-ZnMoO4 nanoparticles as anode material for lithium ion batteries. Materials Letters, 198(3), 4-7. https://doi.org/10.1016/j.matlet.2017.03.160

Fialová, S., Tekel'ová, D., Švajdlenka, E., Potúček, P., Jakubová, K., & Grančai, D. (2014). The variability of secondary metabolites in Mentha × piperita cv. "Perpeta" during the development of inflorescence. Acta Facultatis Pharmaceuticae

Universitatis Comenianae, 61(2), 21-25. https://doi.org/10.2478/afpuc-2014-0012

Jiang, Y. R., Lee, W. W., Chen, K. T., Wang, M. C., Chang, K. H., & Chen, C. C. (2014). Hydrothermal synthesis of β-ZnMoO4 crystals and their photocatalytic degradation of Victoria Blue R and phenol. Journal of the Taiwan Institute of Chemical Engineers, 45(1), 207-218.https://doi.org/10.1016/j.jtice.2013.05.007

Ken Gillman, P. (2011). Review: CNS toxicity involving methylene blue: The exemplar for understanding and predicting drug interactions that precipitate serotonin toxicity. Journal of Psychopharmacology, 25(3), 429-436. https://doi.org/10.1177/0269881109359098

Liebel, F., Kaur, S., Ruvolo, E., Kollias, N., & Southall, M. D. (2012). Irradiation of skin with visible light induces reactive oxygen species and matrix-degrading enzymes. Journal of Investigative Dermatology, 132(7), 1901-1907. https://doi.org/10.1038/jid.2011.476

Low, J., Yu, J., Jaroniec, M., Wageh, S., & Al-Ghamdi, A. A. (2017). Heterojunction Photocatalysts. Advanced Materials, 29(20), 1-20. https://doi.org/10.1002/adma.201601694

Lv, L., Tong, W., Zhang, Y., Su, Y., & Wang, X. (2011). Metastable monoclinic ZnMoO 4: Hydrothermal synthesis, optical properties and photocatalytic performance. Journal of Nanoscience and Nanotechnology, 11(11), 9506-9512. https://doi.org/10.1166/jnn.2011.5269

Mardare, C. C., Tanasic, D., Rathner, A., Müller, N., & Hassel, A. W. (2016). Growth inhibition of Escherichia coli by zinc molybdate with different crystalline structures. Physica Status Solidi (A) Applications and Materials Science, 213(6), 1471-1478. https://doi.org/10.1002/pssa.201532786

Meng, X., Hao, M., Shi, J., Cao, Z., He, W., Gao, Y., … Li, Z. (2017). Novel CuO/Bi2WO6 heterojunction with enhanced visible light photoactivity. Advanced Powder Technology, 28(12), 3247-3256. https://doi.org/10.1016/j.apt.2017.09.036

Nandiyanto, A. B. D., Oktiani, R., & Ragadhita, R. (2019). How to read and interpret ftir spectroscope of organic material. Indonesian Journal of Science and Technology, 4(1), 97-118. https://doi.org/10.17509/ijost.v4i1.15806

Petrović, M., Rančev, S., Velinov, N., Radović Vučić, M., Antonijević, M., Nikolić, G., & Bojić, A. (2021). Triclinic ZnMoO4 catalyst for atmospheric pressure non-thermal pulsating corona plasma degradation of reactive dye; role of the catalyst in plasma degradation process. Separation and Purification Technology, 269(April). https://doi.org/10.1016/j.seppur.2021.118748

Pham, H. L., Nguyen, V. D., Nguyen, V. K., Le, T. H. P., Ta, N. B., Pham, D. C.,Dang, V. T. (2021). Rational design of magnetically separable core/shell Fe3O4/ZnO heterostructures for enhanced visible-light photodegradation performance. RSC Advances, 11(36), 22317-22326. https://doi.org/10.1039/D1RA03468E

Puspitasari, L., Mareta, S., & Thalib, A. (2021). Karakterisasi Senyawa Kimia Daun Mint (Mentha sp.) dengan Metode FTIR dan Kemometrik. Sainstech Farma, 14(1), 5-11. Retrieved from https://ejournal.istn.ac.id/index.php/saintechfarma/article/view/931

Radoor, S., Karayil, J., Jayakumar, A., Parameswaranpillai, J., & Siengchin, S. (2021). Release of toxic methylene blue from water by mesoporous silicalite-1: characterization, kinetics and isotherm studies. Applied Water Science, 11(7), 1-12. https://doi.org/10.1007/s13201-021-01435-z

Reddy, B. J., Vickraman, P., & Justin, A. S. (2018). Investigation of novel zinc molybdate-graphene nanocomposite for supercapacitor applications. Applied Physics A: Materials Science and

Processing, 124(6), 1-9. https://doi.org/10.1007/s00339-018-1793-0

Riwayati, I., Fikriyyah, N., & Suwardiyono, S. (2019). ADSORPSI ZAT WARNA METHYLENE BLUE MENGGUNAKAN ABU ALANG-ALANG (Imperata cylindrica) TERAKTIVASI ASAM SULFAT. Jurnal Inovasi Teknik Kimia, 4(2), 6-11. https://doi.org/10.31942/inteka.v4i2.3016

Sagadevan, S., Fatimah, I., Egbosiub, T. C., Alshahateet, S. F., Lett, J. A., Weldegebrieal, G. K., … Johan, M. R. (2022). Photocatalytic Efficiency of Titanium Dioxide for Dyes and Heavy Metals Removal from Wastewater. Bulletin of Chemical Reaction Engineering & Catalysis, 17(2), 430-450. https://doi.org/10.9767/bcrec.17.2.13948.430-450

Simi, A., & Azeeza, V. (2010). Removal of methylene blue dye using low cost adsorbent. Asian Journal of Chemistry, 22(6), 4371-4376.

Sirirerkratana, K., Kemacheevakul, P., & Chuangchote, S. (2019). Color removal from wastewater by photocatalytic process using titanium dioxide-coated glass, ceramic tile, and stainless steel sheets. Journal of Cleaner Production, 215, 123-130. https://doi.org/10.1016/j.jclepro.2019.01.037

Wang, J. C., Lou, H. H., Xu, Z. H., Cui, C. X., Li, Z. J., Jiang, K., … Shi, W. (2018). Natural sunlight driven highly efficient photocatalysis for simultaneous degradation of rhodamine B and methyl orange using I/C codoped TiO2 photocatalyst. Journal of Hazardous Materials, 360, 356-363. https://doi.org/10.1016/j.jhazmat.2018.08.008

Weldegebrieal, G. K. (2020). Synthesis method, antibacterial and photocatalytic activity of ZnO nanoparticles for azo dyes in wastewater treatment: A review. Inorganic Chemistry Communications, 120(July), 108140. https://doi.org/10.1016/j.inoche.2020.108140

Widiyandari, H., Ketut Umiati, N. A., & Dwi Herdianti, R. (2018). Synthesis and photocatalytic property of Zinc Oxide (ZnO) fine particle using flame spray pyrolysis method. Journal of Physics: Conference Series, 1025(1). https://doi.org/10.1088/1742-6596/1025/1/012004

Xing, X., Xu, X., Wang, J., & Hu, W. (2019). Preparation and inhibition behavior of ZnMoO4/reduced graphene oxide composite for Q235 steel in NaCl solution. Applied Surface Science, 479(February), 835-846. https://doi.org/10.1016/j.apsusc.2019.02.149

Yan, Q., Wang, P., Guo, Y., Chen, Y., Si, Y., & Zhang, M. (2019). Constructing a novel hierarchical ZnMoO4/BiOI heterojunction for efficient photocatalytic degradation of tetracycline. Journal of Materials Science: Materials in Electronics, 30(20), 19069-19076. https://doi.org/10.1007/s10854-019-02264-2

Yulizar, Y., Apriandanu, D. O. B., & Ashna, R. I. (2020). La2CuO4-decorated ZnO nanoparticles with improved photocatalytic activity for malachite green degradation. Chemical Physics Letters, 755(June). https://doi.org/10.1016/j.cplett.2020.137749

Yulizar, Y., Bakri, R., Apriandanu, D. O. B., & Hidayat, T. (2018). ZnO/CuO nanocomposite prepared in one-pot green synthesis using seed bark extract of Theobroma cacao. Nano-Structures and Nano-Objects, 16, 300-305. https://doi.org/10.1016/j.nanoso.2018.09.003

Zhang, Z., Feng, C., Liu, J., & Guo, Z. (2019). Synthesis of ZnMoO4 with different polymorphas anode materials for lithium-ion batteries application. Journal of Materials Science: Materials in Electronics, 30(22), 20213-20220. https://doi.org/10.1007/s10854-019-02405-7